WP15ER-PR(17) 18489

F Riva et al.

Three-dimensional simulations of plasma turbulence in the RFX-mod scrape-off layer and comparison with experimental measurements

Preprint of Paper to be submitted for publication in
Physics of Plasmas

This work has been carried out within the framework of the EUROfusion Consortium and has received funding from the Euratom research and training programme 2014-2018 under grant agreement No 633053. The views and opinions expressed herein do not necessarily reflect those of the European Commission.

Three-dimensional simulations of plasma turbulence in the RFX-mod scrape-off layer and comparison with experimental measurements

Fabio Riva,[1,*] Nicola Vianello,[2] Monica Spolaore,[2] Paolo Ricci,[1]
Roberto Cavazzana,[2] Lionello Marrelli,[2] and Silvia Spagnolo[2]

[1]*École Polytechnique Fédérale de Lausanne (EPFL), Swiss Plasma Center (SPC), CH-1015 Lausanne, Switzerland*

[2]*Consorzio RFX, Corso Stati Uniti 4, 35127 Padova, Italy*

Abstract

The tokamak scrape-off layer (SOL) plasma dynamics is investigated in a circular limiter configuration with a low edge safety factor. Focusing on the experimental parameters of two ohmic tokamak inner-wall limited plasma discharges in RFX-mod [P. Sonato *et al*, Fusion Eng. Des. **74**, 97 (2005)], nonlinear SOL plasma simulations are performed with the GBS code [Ricci *et al*, Plasma Phys. Control. Fusion **54**, 124047 (2012)]. The numerical results are compared with experimental measurements, assessing the reliability of the GBS model in describing the RFX-mod SOL plasma dynamics. It is found that the simulations are able to quantitatively reproduce the RFX-mod experimental measurements of the electron plasma density, electron temperature, and ion saturation current density (j_{sat}) equilibrium profiles. Moreover, there are indications that the turbulent transport is driven by the same instability in the simulations and in the experiment, with coherent structures having similar statistical properties. On the other hand, it is found that the simulation results are not able to correctly reproduce the floating potential equilibrium profile and the j_{sat} fluctuation level. It is likely that these discrepancies are, at least in part, related to simulating only the tokamak SOL region, without including the plasma dynamics inside the LCFS, and to the limits of applicability of the drift approximation. The turbulence drive is then identified from the nonlinear simulations and with linear theory. It results that the inertial drift wave is the instability driving most of the turbulent transport in the considered discharges.

*Electronic address: fabio.riva@epfl.ch

I. INTRODUCTION

Understanding the plasma dynamics in the tokamak scrape-off layer (SOL) is of crucial importance, since phenomena taking place in this region play a fundamental role in determining the overall performance of fusion devices. In fact, the SOL sets the boundary conditions for the tokamak core, it controls the impurity dynamics and the recycling level, and it is responsible of exhausting the tokamak power, thus determining the heat load at the vessel walls [1].

Due to the complex nonlinear phenomena taking place in the SOL, the plasma dynamics in this region is usually investigated numerically, thanks to state-of-the-art simulation codes (see, e.g., Refs. [2–5]). In the present paper we focus on the tokamak limited SOL configuration. Besides being of interest as a stepping stone towards the simulation of more complex experimental scenarios, this configuration has recently attracted large attention since the ITER [6] start-up and ramp-down phases will be performed using the high-field side part of the vacuum vessel as the limiting surface [7, 8].

In the past, extensive theoretical and numerical studies of the instabilities driving the SOL dynamics were performed (see, e.g., Refs. [9–12]). It was found that, in the limited configuration, SOL turbulence is generally driven by drift-waves (DWs) and ballooning modes (BMs) [12, 13]. It was also demonstrated that these linear instabilities typically saturate due to a nonlinear local flattening of the plasma gradient and the resulting removal of the instability drive [14]. These theoretical findings were subsequently validated against experimental measurements taken on a number of tokamaks around the world, such as TCV, MAST, EAST, Alcator C-Mod, ISTTOK, and Tore Supra, showing good agreement between simulations and experimental measurements of plasma turbulence [15–21]. Moreover, using these observations and assuming that resistive BMs drive the SOL turbulence dynamics and that the parallel losses at the vessel are balanced by the turbulent transport, an analytical scaling for the equilibrium pressure gradient length was derived [22, 23]. It was found that this scaling is consistent with measurements taken on a number of experimental devices [24].

The goal of the present paper is to investigate a SOL parameter regime that was not explored earlier and, in general, difficult to access experimentally. More precisely, we investigate the SOL plasma dynamics in a circular limiter configuration with a low safety factor at the last close flux surface (LCFS), $q_{LCFS} \lesssim 3$, for which the SOL turbulence is expected to be clearly

in the inertial DW (InDW) regime [12]. Our study is based on performing SOL turbulence simulations considering two tokamak circular plasma discharges carried out in the RFX-mod experiment [25] with $q_{\rm LCFS} \approx 2, 3$. The RFX-mod device can access such low safety factors thanks to an advanced feedback magnetic boundary control system, which allows stabilizing resistive wall modes and performing plasma discharges with $q_{LCFS} \approx 2$ without disruptions [26]. We then carefully compare the simulation results with RFX-mod experimental measurements and we analyze the nature of the turbulence in the SOL of RFX-mod. The present paper is organized as follows. After the Introduction, in Sec. II we discuss the RFX-mod experimental setup. Then, in Sec. III we describe the simulations of the RFX-mod plasma discharges. In Sec. IV the numerical results are validated against experimental measurements. The instability that drives the SOL plasma dynamics is identified thanks to nonlinear simulations and linear theory in Sec. V. Finally, we report our conclusions in Sec. VI. The presentation of the gradient removal mechanism and its use in evaluating the equilibrium pressure gradient length are discussed in Appendix A.

II. THE EXPERIMENTAL SETUP

The RFX-mod experiment is a flexible toroidal device with major radius $R = 2\,\mathrm{m}$ and minor radius $a = 0.459\,\mathrm{m}$, equipped with a set of 192 actively controlled coils that cover the whole vacuum vessel [25]. While RFX-mod plasma discharges have been performed mainly in the reversed field pinch (RFP) configuration, recent developments allow now operating the device also with magnetic geometries that feature inner-wall limited and diverted ohmic tokamaks [26–28]. Using a toroidal magnetic field on axis $B_\varphi \simeq 0.6\,\mathrm{T}$ and a plasma current up to $I_p \simeq 150\,\mathrm{kA}$, it is possible to perform plasma pulses longer than 1 s with integrated plasma densities $n_e \geq 10^{19}\,\mathrm{m}^{-3}$ and core electron temperatures $T_e \geq 500\,\mathrm{eV}$.

In the following we consider two circular inboard-limited ohmic L-mode deuterium plasma discharges (#38373 and #38413) carried out in the RFX-mod device with a toroidal magnetic field on axis $B_\varphi = 0.54\,\mathrm{T}$ and plasma currents $I_p = 150\,\mathrm{kA}$ and $I_p = 100\,\mathrm{kA}$. These two plasma currents correspond to $q_{\rm LCFS} = 2$ and $q_{\rm LCFS} = 3$, respectively. The plasma densities and electron temperatures at the LCFS for the two discharges are $n_{e0} = 7.7 \times 10^{17}, 2.0 \times 10^{17}\,\mathrm{m}^{-3}$ and $T_{e0} = 16, 19\,\mathrm{eV}$, respectively, and correspond to the two normalied plasma collisionalities $\nu^* = L_\parallel/\lambda^{mfp} = 6.9, 1.3$, where $L_\parallel = 2\pi q_{LCFS} R$ is the parallel

connection length and λ^{mfp} the electron mean free path.

The experimental measurements illustrated in the following of this paper are obtained using the U-probe installed in RFX-mod. This probe consists of two boron nitride arms, each of them equipped with 25 electrostatic pins [29, 30]. Some of the pins are used as a five-pin triple probe [31], allowing simultaneous measurements of ion saturation, I_{sat}, plasma density, n, electron temperature, T_e, and floating potential, V_{fl}, with time resolution of $0.2\,\mu$s. The U-probe is located at a fixed radial position at the outward equatorial midplane, with its arms in the horizontal direction. In order to obtain measurements at different radial locations, the plasma column is slowly shifted towards the inner wall of the device during the discharge, while keeping a constant edge safety factor. We note that the measurements are obtained at approximately 2.8 cm from the vessel wall. Additionally, we also note that the experimental measurements related to the #38373 plasma discharge we use for the present validation are taken only in between sawtooth crashes. This leads to a reduced number of measurements for the considered time traces (20'000 measurements) available for the analysis of the #38373 discharge (approximately a factor ten less with respect to the #38413 discharge, for which we have 175'000 measurements).

III. GBS SIMULATIONS OF THE RFX-MOD SOL

Because of its high collisionality, the tokamak SOL region is generally studied by employing a plasma fluid description, such as the Braginskii fluid model [32]. Moreover, since the SOL turbulent time scales are much slower than the ion cyclotron time, and the perpendicular (to $\mathbf{B}$) scale lengths are longer than the ion Larmor radius, the drift approximation can be applied to simplify the fluid model, thus obtaining a set of drift-reduced Braginskii equations useful to describe the SOL plasma dynamics [33]. We consider this model also for the present study, althought the conditions for the applicability of the fluid model are marginally satisfied for the RFX-mod #38413 plasma discharge. Neglecting electromagnetic effects as suggested in Ref. [34], since $\beta_e R/L_p \leq 10^{-3}$ in the RFX-mod SOL (β_e is the plasma to magnetic pressure ratio and L_p the equilibrium pressure gradient length), assuming an infinite aspect ratio (the influence of finite aspect ratio effects on SOL plasma dynamics is studied in Ref. [35]) and cold ions (no ion temperature measurements are available on RFX-mod for these discharges, the impact of ion temperature effects on SOL turbulence

is investigated in Ref. [36]), and employing the Boussinesq approximation to simplify the vorticity equation (the validity of this assumption in modelling the SOL plasma dynamics is discussed in Refs. [37–39]), the drift-reduced Braginskii equations in normalized units are written as

$$\partial_t n = - R_0 \{\phi, n\} + 2 [C(p_e) - nC(\phi)] - \nabla_\parallel \left(n v_{\parallel e}\right) + D_n \nabla_\perp^2 n + S_n, \tag{1}$$

$$\partial_t \omega = - R_0 \{\phi, \omega\} + \frac{2}{n} C(p_e) - v_{\parallel i} \nabla_\parallel \omega + \frac{1}{n} \nabla_\parallel j_\parallel + \frac{1}{3n} C(G_i) + D_\omega \nabla_\perp^2 \omega, \tag{2}$$

$$\begin{aligned} \partial_t v_{\parallel e} = &- R_0 \left\{\phi, v_{\parallel e}\right\} + \frac{m_i}{m_e} \left[\nabla_\parallel \phi - \frac{1}{n} \nabla_\parallel p_e - 0.71 \nabla_\parallel T_e + \nu j_\parallel - \frac{2}{3n} \nabla_\parallel G_e\right] \\ &- v_{\parallel e} \nabla_\parallel v_{\parallel e} + D_{v_{\parallel e}} \nabla_\perp^2 v_{\parallel e}, \end{aligned} \tag{3}$$

$$\partial_t v_{\parallel i} = - R_0 \left\{\phi, v_{\parallel i}\right\} - v_{\parallel i} \nabla_\parallel v_{\parallel i} - \frac{1}{n} \nabla_\parallel p_e - \frac{2}{3n} \nabla_\parallel G_i + D_{v_{\parallel i}} \nabla_\perp^2 v_{\parallel i}, \tag{4}$$

$$\begin{aligned} \partial_t T_e = &- R_0 \{\phi, T_e\} + \frac{4}{3} T_e \left[\frac{7}{2} C(T_e) + \frac{T_e}{n} C(n) - C(\phi)\right] - v_{\parallel e} \nabla_\parallel T_e + \nabla_\parallel \left(\chi_{\parallel e} \nabla_\parallel T_e\right) \\ &+ \frac{2}{3} T_e \left[0.71 \nabla_\parallel v_{\parallel i} - 1.71 \nabla_\parallel v_{\parallel e} + 0.71 \left(\frac{v_{\parallel i} - v_{\parallel e}}{n}\right) \nabla_\parallel n\right] + D_{T_e} \nabla_\perp^2 T_e + S_{T_e}, \end{aligned} \tag{5}$$

where $\omega = \nabla_\perp^2 \phi$ is the plasma vorticity, m_i/m_e the ion to electron mass ratio, R_0 is the normalized RFX-mod major radius, $j_\parallel = n(v_{\parallel i} - v_{\parallel e})$ the parallel current, $p_e = nT_e$ the electron plasma pressure, ν the normalized Spitzer resistivity, and $\chi_{\parallel e}$ the parallel electron thermal conductivity. The density and electron temperature sources S_n and S_{T_e} describe the plasma outflow from the core. The expressions of the two terms representing the ion and electron gyroviscous contributions are given by $G_i = -\eta_{0i} \left[2\nabla_\parallel v_{\parallel i} + C(\phi)\right]$ and $G_e = -\eta_{0e} \left[2\nabla_\parallel v_{\parallel e} - C(p_e)/n + C(\phi)\right]$, respectively, where η_{0i} and η_{0e} are the normalized gyroviscous coefficients [32]. The Poisson brackets are defined as $\{\phi, A\} = \mathbf{b} \cdot (\nabla\phi \times \nabla A)$, the curvature operator as $C(A) = B/2 [\nabla \times (\mathbf{b}/B)] \cdot \nabla A$, the parallel gradient as $\nabla_\parallel A = \mathbf{b} \cdot \nabla A$, and the perpendicular Laplacian as $\nabla_\perp^2 A = -\nabla \cdot [\mathbf{b} \times (\mathbf{b} \times \nabla A)]$, with $\mathbf{b}$ the unit vector parallel to $\mathbf{B}$ and $A = n, \omega, \phi, v_{\parallel i}, v_{\parallel e}, T_e$. Small perpendicular diffusion terms of the form $\mathcal{D}_A(A) = D_A \nabla_\perp^2 A$ are added for numerical stability reasons. Unless specified otherwise, in the present paper all quantities are normalized to (tilde denotes a physical quantity in SI units): $t = \tilde{t} / \left(\tilde{R}/\tilde{c}_{s0}\right)$, $n = \tilde{n}/\tilde{n}_0$, $T_e = \tilde{T}_e/\tilde{T}_{e0}$, $\phi = e\tilde{\phi}/\tilde{T}_{e0}$, $v_{\parallel e} = \tilde{v}_{\parallel e}/\tilde{c}_{s0}$, $v_{\parallel i} = \tilde{v}_{\parallel i}/\tilde{c}_{s0}$, $B = \tilde{B}/\tilde{B}_0$, $R_0 = \tilde{R}/\tilde{\rho}_{s0}$, $\nu = \left(e^2 \tilde{n}_0 \tilde{R}\right) / \left(m_i \tilde{\sigma}_\parallel \tilde{c}_{s0}\right)$, where $\tilde{\sigma}_\parallel$ is the parallel conductivity, $\tilde{n}_0$, $\tilde{T}_{e0}$ and $\tilde{B}_0$ are reference density, temperature, and magnetic field, $\tilde{R}$ is the tokamak major radius, and $\tilde{c}_{s0}$ and $\tilde{\rho}_{s0}$ are given by $\tilde{c}_{s0} = \sqrt{\tilde{T}_{e0}/m_i}$ and $\tilde{\rho}_{s0} = \tilde{c}_{s0} m_i / \left(e\tilde{B}_0\right)$. Distances perpendicular to $\mathbf{B}$ are normalized to $\tilde{\rho}_{s0}$, while parallel distances are normalized to $\tilde{R}$.

Equations (1)-(5) are solved with GBS, a code developed in the last few years to simulate plasma turbulence in the open field region of basic plasma physics experiments and magnetic confinement devices, evolving the full plasma profiles without any separation between equilibrium and perturbation quantities [3, 40]. To develop the GBS code, increasingly complex magnetic configurations were considered. First, the code was developed to describe the plasma dynamics in basic plasma physics experiments, in particular linear devices such as LAPD [41] and simple magnetized toroidal devices such as TORPEX [42–44]. GBS was then extended to the tokamak geometry, and it is now able to model the tokamak SOL region in limited plasmas [12, 14, 22, 34]. To solve Eqs. (1)-(5), GBS makes use of the toric ($y = a\theta, x = r, z = \varphi$) coordinate system, with θ and φ the poloidal and toroidal angles, and r a flux coordinate. Consequently, considering circular magnetic flux surfaces in the infinite aspect ratio limit and assuming no magnetic shear (a discussion of the impact of these assumptions on DWs and BMs is presented in Refs. [12, 13]), the differential operators can be rewritten as $\{\phi, A\} = \partial_y\phi\partial_x A - \partial_x\phi\partial_y A$, $C(A) = \sin(\theta)\partial_x A + \cos(\theta)\partial_y A$, $\nabla_\parallel A = \partial_z A + a\partial_y A/q$, and $\nabla_\perp^2 A = \partial_x^2 A + \partial_y^2 A$, with $q = q_{LCFS}$. Note that the poloidal angle is defined such that $\theta = 0$ and $\theta = 2\pi$ at the outer midplane.

The drift-reduced Braginskii system, Eqs. (1)-(5), is closed by a set of boundary conditions describing the plasma properties at the magnetic pre-sheath entrance [45]. Within the assumptions used in this section, these boundary conditions are written as

$$v_{\parallel i} = \pm\, c_s, \tag{6}$$

$$v_{\parallel e} = \pm\, c_s \exp\left(\Lambda - \phi/T_e\right), \tag{7}$$

$$\partial_y T_e = 0, \tag{8}$$

$$\partial_y n = \mp\, \frac{n}{c_s}\partial_y v_{\parallel i}, \tag{9}$$

$$\omega = -\left(\partial_y v_{\parallel i}\right)^2 \mp c_s\partial_y^2 v_{\parallel i}, \tag{10}$$

$$\partial_y \phi = \mp\, c_s\partial_y v_{\parallel i}, \tag{11}$$

where $\Lambda = \log\sqrt{m_i/(2\pi m_e)} \simeq 3$ for deuterium plasmas. Here the upper signs apply to the case of magnetic field directed towards the wall, while the lower ones apply to the opposite case. Equations (1)-(11) are solved using a second-order finite difference scheme in the spatial dimensions, except for the Poissons brackets, which are discretized with a second order Arakawa scheme [46]. Time is advanced using a standard fourth-order Runge-Kutta

scheme. For a more detailed description of GBS we refer to Refs. [3, 40].

Focusing on a circular plasma with a toroidal limiter located at the high-field side, we perform two nonlinear GBS simulations based on the RFX-mod experimental parameters R, q_{LCFS}, n_{e0}, and T_{e0}. For the two plasma discharges #38373 and #38413 these parameters lead to the normalized plasma resistivities $\nu = 0.005, 0.001$, the normalized major radii $R_0 = 1872, 1716$, and the poloidal domain sizes $L_y = 2700, 2470$. In addition, we consider a reduced ion to electron mass ratio $m_i/m_e = 800$, a reduced normalized parallel electron thermal conductivity $\chi_{\parallel e} = 2$, and the normalized perpendicular diffusion coefficients $D_A = 5$. The particle and temperature sources, used to mimic the plasma outflow from the core, are assumed poloidally and toroidally constant, with radial dependence $S_n(x) \propto S_{T_e} \propto \exp\left[-(x-a)^2/\sigma^2\right]$, being $\sigma = 2.5$. The radial domain extends from the inner radius $x_i = a - 30$ to the outer radius $x_o = a + 70$ in both simulations. Since a set of first-principle boundary conditions describing the plasma interaction with the outer wall and the interface between the SOL and the core does not exist yet, ad hoc boundary conditions are applied at x_i and x_o, with Neumann's boundary conditions used for n, $v_{\parallel e}$, $v_{\parallel i}$, and T_e, and Dirichlet's boundary conditions for ω and ϕ. To mitigate the impact of these boundary conditions on the simulation results, the two regions extending from x_i to $x = a$, and from $x = a + 55$ to x_o are considered as buffers and are not included in the analysis of the results. We note that, because of the necessary rather large numerical grids $(N_x, N_y, N_z) = (128, 1279, 320)$, $(128, 1279, 212)$, with N_x, N_y, and N_z the number of points in the radial, poloidal, and toroidal directions, the two simulations discussed herein are extremely expensive in terms of computational resources (approximately one million CPU hours each). The reduced mass ratio and parallel electron thermal conductivity are consequently used to considerably decrease the cost of the simulations. The impact of a reduced mass ratio on the results is investigated in Sec. V B by means of linear simulations. We also note that, while in the experiment the plasma current and the toroidal magnetic field are in the same direction, we use a current that is in the opposite direction to the magnetic field in the GBS simulations. We defer the detailed analysis of the impact of the sign of plasma current on SOL turbulence to a future study.

The equilibrium pressure gradient length $L_p = -p_e/\nabla p_e$ is directly evaluated from nonlinear simulations by computing the averaged radial p_e profile $p_e(y, x) = \langle p_e(y, x, z, t)\rangle_{z,t}$, where $\langle -\rangle_{z,t}$ denotes averaging over z and t, and fitting $p_e(y, x)$ at fixed y between $x = a$

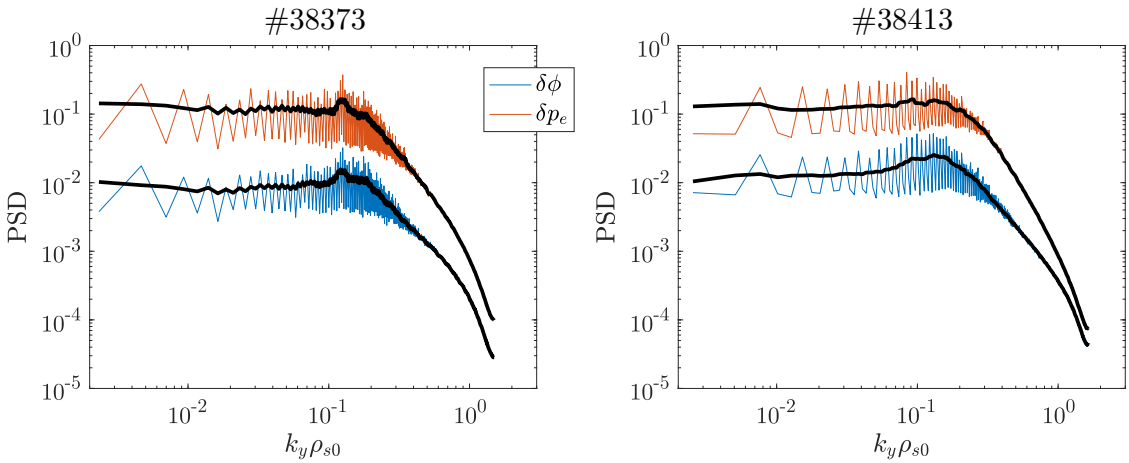

FIG. 1: PSD of $\delta\phi$ (blue lines) and δn (red lines) for the two simulations of the RFX-mod plasma discharges #38373 (left) and #38413 (right) at the outer midplane, at approximately 2 cm from the LCFS. The black lines denote a smoothing of the PSD profiles.

and $x = a + 55$ assuming $p_e(y, x) \propto \exp[-(x - a)/L_p(y)]$. For the two plasma discharges #38373 and #38413 we find at the outer midplane $L_p(0) = 31$ and $L_p(0) = 37$, respectively. Moreover, computing in the nonlinear simulations the power spectral density (PSD) of the p_e and ϕ fluctuations, δp_e and $\delta\phi$, it is possible to estimate the poloidal wave number of the mode that drives most of the turbulent transport (see Fig. 1). For the two plasma discharges considered herein we find $k_y \approx 0.1 - 0.2$.

IV. VALIDATION OF THE GBS SIMULATIONS AGAINST EXPERIMENTAL MEASUREMENTS

In order to assess the reliability of the drift-reduced Braginskii model and of the GBS simulations, we compare the nonlinear numerical results with RFX-mod experimental measurements. We remark that the plasma dynamics inside the LCFS is neglected in the simulations considered herein. Therefore, we expect a better agreement between simulation results and experimental measurements in the far SOL than in the near SOL. Note that the results illustrated in the present section are in SI units.

First, we present in Fig. 2 the experimental and numerical radial equilibrium profiles of n, T_e, j_{sat}, and V_{fl} for the two RFX-mod discharges discussed above (we evaluate $j_{sat} = enc_s/2$ and $V_{fl} = \phi - \Lambda T_e/e$ in the simulations). According to the results presented in Ref. [47], we

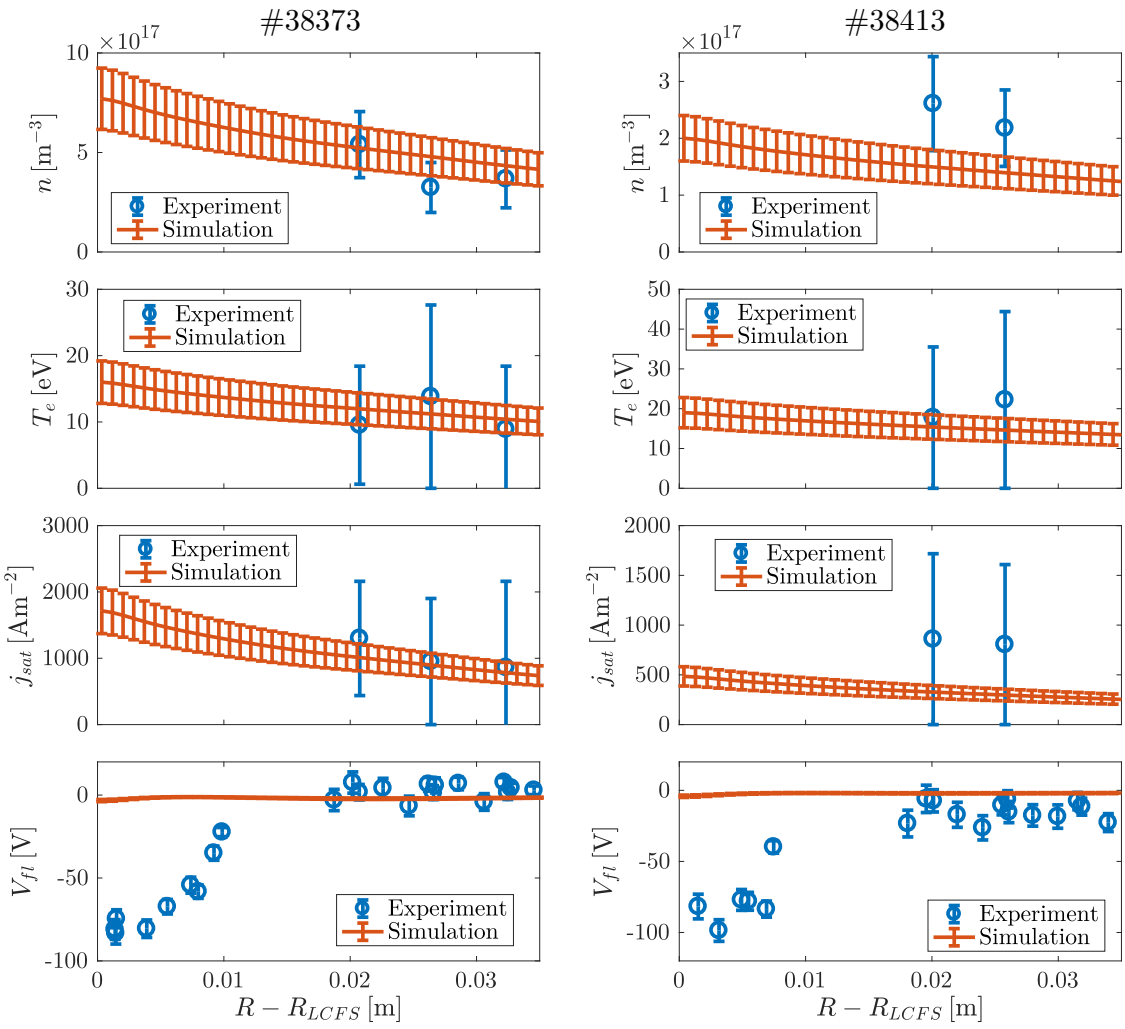

FIG. 2: Experimental (blue circles) and simulation (red lines) radial equilibrium profiles of plasma density (first row), electron temperature (second row), ion saturation current density (third row), and floating potential (fourth row), for the two RFX-mod plasma discharges #38373 (left column) and #38413 (right column).

assume a 20% relative discretization error affecting the simulation equilibrium profiles and we neglect other sources of uncertainties. We observe that the equilibrium radial profiles of n, T_e, and j_{sat} obtained from the nonlinear simulations of both discharges are consistent with the experimental results within the estimated uncertainties. We also note that, since the experimental uncertainties are rather large, it is not possible to reliably estimate the experimental n and T_e equilibrium gradient lengths. Concerning V_{fl}, the simulation results do not agree with the experimental measurements, in particular in the proximity of the LCFS. As a matter of fact, while the experimental measurements are in agreement with observa-

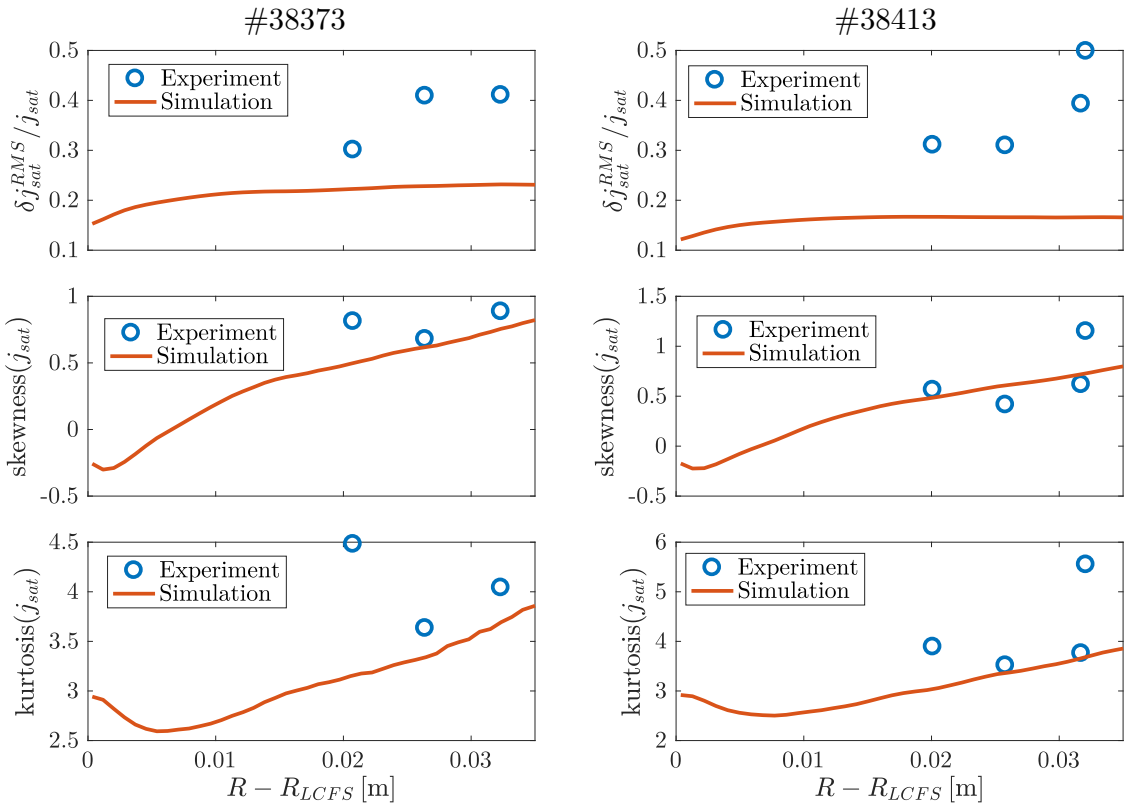

FIG. 3: Experimental (blue circles) and simulation (red lines) radial profiles of $\delta j_{sat}^{RMS}/j_{sat}$ (first row), j_{sat} skewness (second row), and j_{sat} kurtosis (third row), for the two RFX-mod plasma discharges #38373 (left column) and #38413 (right column).

tions in other devices (see, e.g., Ref. [48]), with a strong drop of V_{fl} in the proximity of the LCFS extending for a few millimeters in the SOL, the simulation profiles are flatter, with an absolute value of V_{fl} closer to zero. This discrepancy is probably related to simulating only the open field line region of RFX-mod, since the plasma dynamics close to the LCFS plays an important role in setting V_{fl} in the near SOL [49], and to neglecting ion temperature effects.

In Fig. 3 we compare the experimental root-mean-square (RMS) values of j_{sat} fluctuations, δj_{sat}^{RMS}, normalized to the equilibrium j_{sat}, with the simulation results. We observe that the simulations underestimate the j_{sat} fluctuations approximately by a factor of two in both considered discharges. In Fig. 3 we also display the skewness and the kurtosis of the experimental and numerical j_{sat} time traces. For these quantities the simulation results show a better agreement with the experimental measurements than for δj_{sat}^{RMS}. In particular, the simulation results display a j_{sat} skewness close to zero in the proximity of the LCFS and

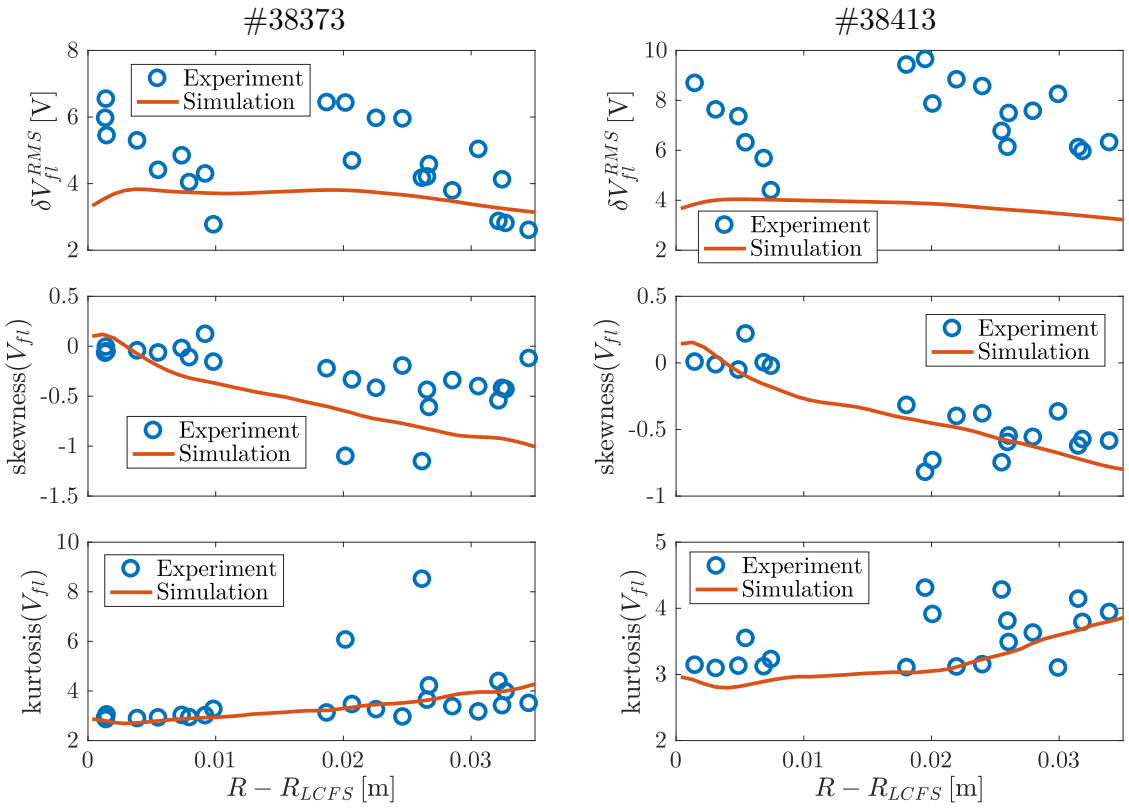

FIG. 4: Experimental (blue circles) and simulation (red lines) radial profiles of δV_{fl}^{RMS} (first row), V_{fl} skewness (second row), and V_{fl} kurtosis (third row), for the two RFX-mod plasma discharges #38373 (left column) and #38413 (right column).

monotonically increasing in the SOL, in agreement with previous experimental SOL investigations [50–52].

In Fig. 4 we present the radial profiles of the V_{fl} fluctuation RMS values, δV_{fl}^{RMS}, and of the V_{fl} skewness and kurtosis. Concerning the RMS values, we observe an almost radial constant level of fluctuations both in the simulations and in the experimental measurements. However, while the numerical results display a quite good quantitative agreement with the RFX-mod experimental measurements for the #38373 discharge, the agreement worsen considering the discharge with lower plasma collisionality. The V_{fl} skewness monotonically decreases in the SOL both for the simulations and for the RFX-mod experimental measurements, with good quantitative agreement between the two quantities. Finally, concerning the V_{fl} kurtosis, we observe good qualitative agreement for both discharges, with an almost constant value close to three, except for $R - R_{LCFS} > 2.5\,\mathrm{cm}$, where the kurtosis is larger. We note that a comparison of the V_{fl} moments between simulations and experimental measurements is

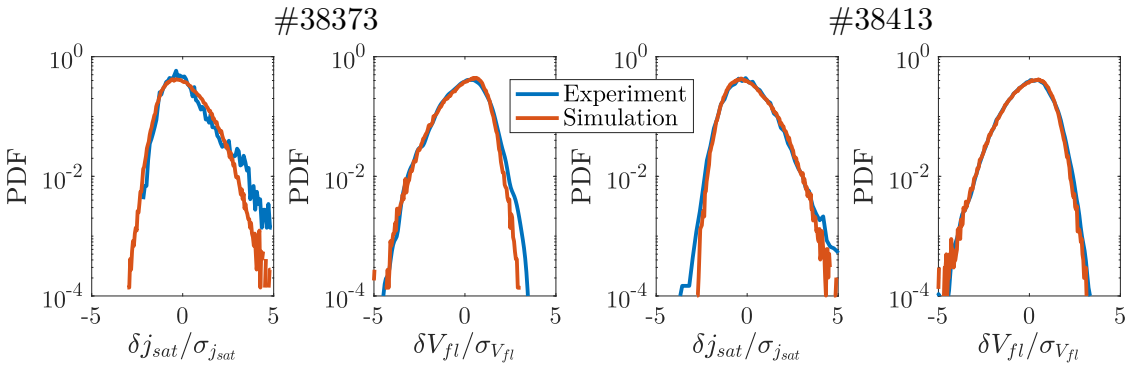

FIG. 5: Experimental (blue lines) and simulation (red lines) PDF of δj_{sat} (first and third column) and δV_{fl} (second and fourth column) normalized to their standard deviation. The results are evaluated approximately at 2 cm from the LCFS and are displayed for the two RFX-mod plasma discharges #38373 (first and second columns) and #38413 (third and fourth columns).

also discussed in Ref. [53] considering TORPEX plasma discharges. Considerably larger discrepancies between numerical results and experimental measurements were found in that case, probably due to the presence of fast electrons, resulting from the source operating at the electron cyclotron resonance.

Our observations on the agreement of j_{sat} and V_{fl} skewness and kurtosis are confirmed by comparing the numerical and experimental probability density functions (PDF) corresponding to j_{sat} and V_{fl} fluctuations, δj_{sat} and δV_{fl}, normalized to their standard deviation in the far SOL, at approximately 2 cm from the LCFS, as shown in Fig. 5. We observe that the simulation results are in good agreement with experimental measurements for both physical quantities and for both discharges. The δj_{sat} PDF displays a positive skewness, while the δV_{fl} PDF is negatively skewed. We note that small differences are observed between experimental measurements and simulation results in the PDF tails, particularly for the plasma discharge #38373. This could be due to intermittent events, originated inside the LCFS, that are not taken into account in the simulations. However, these differences are too small to explain the different level of j_{sat} fluctuations, and they allow us to conclude that the different levels of fluctuations between simulations and experimental measurements are not related to coherent intermittent events, which would strongly affect the PDF tails.

To gain a deeper insight on the nature of the instability driving most of the SOL turbulent transport, in Fig. 6 we compare the experimental joint probabilities between δj_{sat} and δV_{fl}

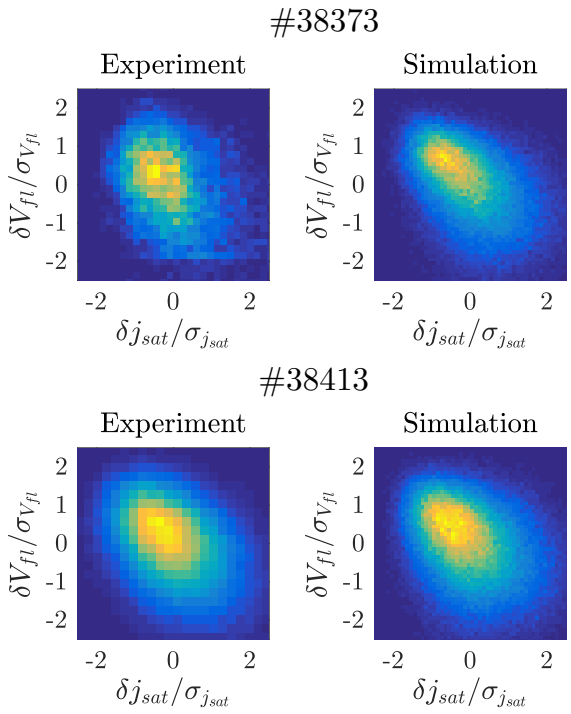

FIG. 6: Experimental (first column) and simulation (second column) joint probabilities of δj_{sat} and δV_{fl} normalized to their standard deviation. The results are evaluated approximately at 2 cm from the LCFS and are displayed for the two RFX-mod plasma discharges #38373 (first row) and #38413 (second row).

at approximately 2 cm from the LCFS, normalized to their standard deviation, with the simulation results. A good qualitative agreement between experimental measurements and simulation results is found, with $\delta j_{sat}/\sigma_{j_{sat}}$ and $\delta V_{fl}/\sigma_{V_{fl}}$ showing moderate anticorrelation. For the analysis of the equilibrium profiles and fluctuation properties, it emerges that the major difference between experimental measurements and simulations lies in the level of j_{sat} fluctuations. We explore the reason of this discrepancy in Fig. 7, where we display the numerical and experimental PSD of j_{sat} and V_{fl}. We observe that for both discharges and for both quantities the PSD monotonically decreases for $f \gtrsim 10$ kHz, in agreement with previous observations [20]. However, the simulation PSD is smaller than the experimental one, particularly for the #38413 discharge, whose plasma collisionality is smaller, consistently with the δj_{sat}^{RMS} and δV_{fl}^{RMS} observations. In addition, while in the simulations the j_{sat} and V_{fl} spectral-slopes, α_{jsat} and α_{Vfl}, are very similar, with $\alpha_{jsat} \simeq \alpha_{Vfl} \simeq -2.4$ for $10\,\text{kHz} \lesssim f \lesssim 100\,\text{kHz}$ and $\alpha_{jsat} \simeq \alpha_{Vfl} \simeq -4.1$ for $f \gtrsim 100$ kHz, in the experiment we

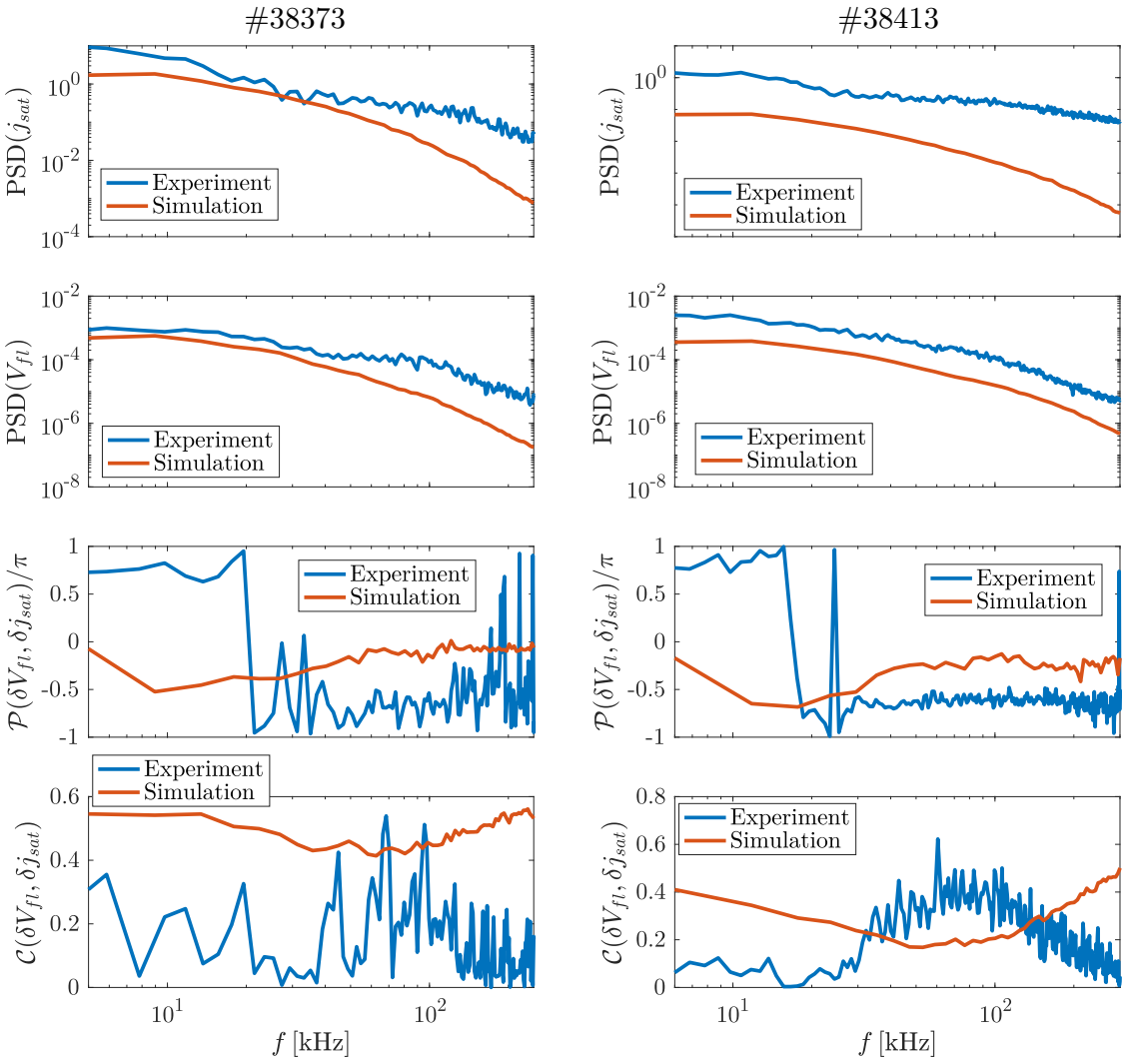

FIG. 7: Experimental (blue lines) and simulation (red lines) profiles of the j_{sat} (first row) and V_{fl} (second row) PSD, and of the phase shift (third row) and the coherence (fourth row) between δj_{sat} and δV_{fl}, for the two RFX-mod plasma discharges #38373 (left column) and #38413 (right column).

have $\alpha_{jsat} \simeq \alpha_{Vfl} \simeq -1.0$ for $10\,\mathrm{kHz} \lesssim f \lesssim 100\,\mathrm{kHz}$ and $\alpha_{jsat} \simeq -2.5$ and $\alpha_{Vfl} \simeq= -2.9$ for $f \gtrsim 100\,\mathrm{kHz}$. We note that $\alpha_{jsat} \neq \alpha_{Vfl}$ is observed also in other experimental devices (see, e.g., Ref. [54]). In Fig. 7 we also display the phase shift and the coherence between j_{sat} and V_{fl} fluctuations. First, we note that the experimental measurements are noisier for the #38373 discharge because of the presence of sawtooth instabilities and of the resulting lower temporal statistics used for the analysis. We also observe that the phase shift between δV_{fl} and δj_{sat}, $\mathcal{P}(\delta V_{fl}, \delta j_{sat})$, resulting from the nonlinear simulations is in better

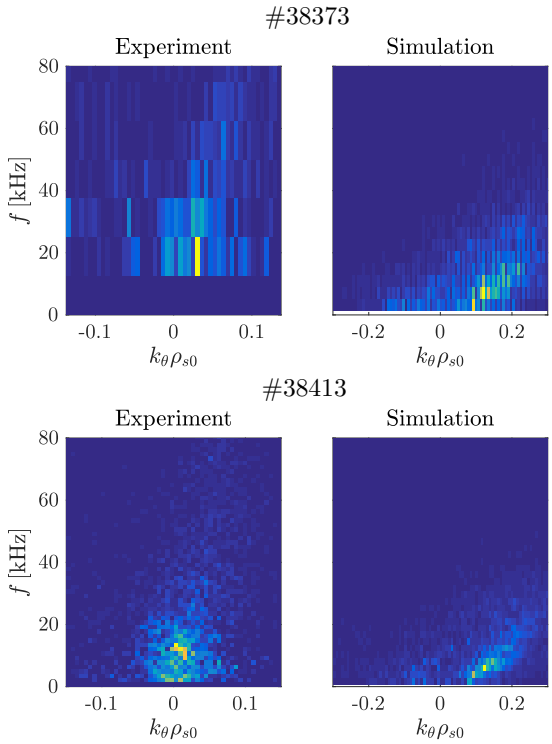

FIG. 8: Experimental (first column) and simulation (second column) $S(k_\theta, f)$ spectra obtained from V_{fl} time-traces for the two RFX-mod plasma discharges #38373 (first row) and #38413 (second row).

agreement with experimental measurements for $f \gtrsim 20\,\mathrm{kHz}$ than it is at low frequencies. As a matter of fact, in the simulations we find $\mathcal{P}(\delta V_{fl}, \delta j_{sat}) < 0$ at all frequencies, while in the experiment $\mathcal{P}(\delta V_{fl}, \delta j_{sat}) > 0$ for $f \lesssim 20\,\mathrm{kHz}$. This discrepancy at low frequencies seems related to incoherent experimental fluctuations, as shown in the last row of Fig. 7. In fact, the simulation results display a quite strong coherence between δj_{sat} and δV_{fl} at all frequencies, while the experimental measurements show a lower coherence, particularly at low frequencies. Overall, the results presented in Fig. 7 indicate a better agreement between simulations and experimental measurements in the frequency range $10\,\mathrm{kHz} \lesssim f \lesssim 100\,\mathrm{kHz}$, where the coherence between δj_{sat} and δV_{fl} is higher, while the agreement worsen at low and high frequencies, with the RFX-mod measurements dominated by incoherent fluctuations. To further investigate the discrepancies observed between simulations and experimental measurements, in Fig. 8 we display the $S(k_\theta, f)$ spectra obtained from the V_{fl} time traces at $R - R_{LCFS} \simeq 2\,\mathrm{cm}$ and related to the two plasma discharges #38373 and #38413. We note that, while the spectra obtained from the V_{fl} experimental measurements are evaluated ac-

cording to the two-point correlation technique described in Ref. [55], the simulation results are obtained computing the Fourier transform of the V_{fl} time signals along t and y. In Fig. 8 we observe that the modes are mainly rotating in the ion diamagnetic direction, both in the experiment and in the simulations. However, while in the experiment the dominant modes have $k_\theta \rho_{s0} \lesssim 0.03$, for the simulations $0.1 \leq k_\theta \rho_{s0} \leq 0.2$, as also shown in Sec. III. We note that, assuming a linear relation between k and f, in the simulations we obtain $k_\theta \gtrsim 1/\rho_{s0}$ for $f \gtrsim 100\,\mathrm{kHz}$. Since the drift approximation is not justified for $k_\theta \rho_{s0} \gtrsim 1$, and $k_\theta \rho_{s0} = 1$ corresponds approximately to the maximum wave number resolved by the grids used for the present simulations, we infer that the increasing discrepancy observed for $f \gtrsim 100\,\mathrm{kHz}$ in the PSD may be related to the limits of the drift-reduced Braginskii model and to the simulation finite grid resolution.

In summary, the GBS model is able to qualitatively reproduce most of the RFX-mod experimental measurements, with the noteworthy exception of δj_{sat} and, in general, a better agreement for the RFX-mod plasma discharge #38373, whose plasma collisionality is higher than in the #38413 discharge. Since the δj_{sat} and δV_{fl} phase shift and joint probability agree between simulation results and experimental measurements at the frequencies where the fluctuations are more coherent, we infer that the nature of the SOL turbulent transport in the simulations and in the experiment should be the same, with coherent structures having similar statistical properties.

The differences observed in the V_{fl} radial profile and in the level of j_{sat} fluctuations may be, at least in part, related to simulating only the tokamak SOL region, neglecting the plasma dynamics inside the LCFS. As a matter of fact, we note that previous tests performed considering GBS simulations of ISSTOK [56] indicate an increase of $\delta j_{sat}^{RMS}/j_{sat}$ up to 30% when the plasma dynamics inside the LCFS is included in the simulations. In addition, sensitivity tests pointed out that δj_{sat}^{RMS} depends on the plasma resistivity, with δj_{sat}^{RMS} increasing by approximately 15% when increasing ν by a factor ten.

V. IDENTIFICATION OF THE INSTABILITY DRIVING THE SOL TRANSPORT

Previous investigations of the SOL plasma dynamics indicate DWs and BMs as the main instabilities driving SOL turbulent transport [12, 34, 57]. BMs are interchange-like modes,

driven unstable, in the presence of plasma resistivity and electron inertia, by magnetic curvature and pressure gradients pointing in the same direction [11, 58–61]. DWs are due to an $\mathbf{E}\times\mathbf{B}$ convection of the plasma pressure when electron adiabaticity is broken by resistivity or finite electron mass, leading respectively to resistive DWs (RDW) and InDWs [62–66].
Past works show that q_{LCFS} and ν strongly affect the SOL turbulent regime. In particular, it is demonstrated that it exists a threshold value of ν below which a transition from resistive BMs (RBM) to InDWs is observed, and this threshold value increases with the decrease of the edge safety factor [12]. While in typical tokamak conditions the SOL is expected to be in the RBM regime or marginally in the DW regime, for the parameters considered herein turbulence is expected to be clearly in the InDW regime [12].
The comparison of the nonlinear simulations against RFX-mod experimental measurements in Sec. IV shows good agreement for most of the considered quantities. This comparison allows us to infer that the SOL turbulent transport is mostly driven by the same instability in the experiment and in the simulations. Consequently, in the following of this section we investigate the nature of the instability that drives most of the SOL turbulent transport in the RFX-mod plasma discharges #38373 and #38413 by using nonlinear simulations and, also, the linear theory.

A. Nonlinear simulations

In order to identify the instability that drives most of the RFX-mod SOL turbulent transport, we proceed as follows. Considering the plasma discharge #38373, we perform three nonlinear simulations solving (i) the "full" GBS model, Eqs. (1)-(5), (ii) the "BM" model, considering Eqs. (1)-(5) where we neglect the diamagnetic term in the Ohm's equation, i.e. we simplify Eq. (3) as

$$\partial_t v_{\parallel e} = -\frac{R}{\rho_{s0}}\left\{\phi, v_{\parallel e}\right\} + \frac{m_i}{m_e}\left[\nabla_\parallel \phi + \nu j_\parallel - \frac{2}{3n}\nabla_\parallel G_e\right] - v_{\parallel e}\nabla_\parallel v_{\parallel e} + D_{v_{\parallel e}}\nabla_\perp^2 v_{\parallel e}, \tag{12}$$

and (iii) the "DW" model, where we neglect the pressure curvature term in the vorticity equation of the "full" GBS model, which corresponds to rewriting Eq. (2) as

$$\partial_t \omega = -\frac{R}{\rho_{s0}}\left\{\phi, \omega\right\} - v_{\parallel i}\nabla_\parallel \omega + \frac{1}{n}\nabla_\parallel j_\parallel + \frac{1}{3n}C\left(G_i\right) + D_\omega \nabla_\perp^2 \omega. \tag{13}$$

For each simulation we then compute $L_p(y)$ following the procedure described in Sec. III. The values of $L_p(y)$ thus obtained are shown in Fig. 9 for the three models. We observe that

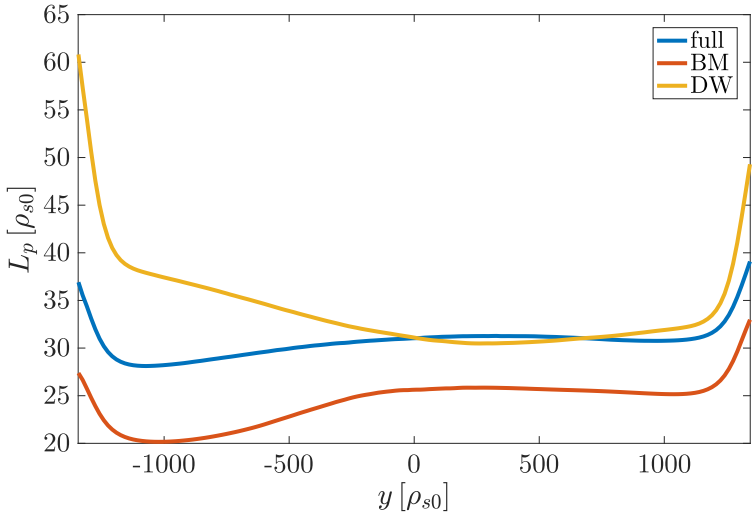

FIG. 9: Profiles of L_p as function of y based on the RFX-mod discharge #38373, solving the "full" GBS model, Eqs. (1)-(5) (blue line), the "BM" model (red line), and the "DW" model (yellow line).

the "full" and the "DW" models lead to quite similar L_p for $y > 0$, while L_p is larger for $y < 0$ in the "DW" simulations, particularly in the proximity of the limiter. This is probably due to the stabilizing effect of magnetic curvature on SOL turbulence at the tokamak high-field side. On the other hand, the value of L_p for the "BM" model is smaller than in the original simulation for all y. This suggests that DWs are driving most of the SOL turbulent transport, and therefore are responsable of the flattening of the pressure profile, in agreement with the expectations in Ref. [12].

We note that, because of the extremely high computational cost of the simulations, we did not perform simulations with the "BM" and "DW" models for the #38413 discharge. However, according to Ref. [12], the same nature of the SOL turbulence is expected for the two discharges considered herein.

B. Linear instabilities

As a confirmation of the nature of the turbulent transport identified by using the nonlinear simulations, we consider the linear properties of the instability dominating the SOL plasma dynamics. This approach allows us also to disentangle more easily the role of resistivity and electron inertia and to study the realistic ion to electron mass ratio not accessible by the nonlinear simulations.

First, in order to deduce a linear model useful for identifying the SOL turbulent regimes, we introduce the flux-tube ($X = r, Y = a\alpha/q, Z = qR_0\theta$) coordinate system, where $\alpha = \varphi - q(r)\theta$ is a field line label. Equations (1)-(5) are then expressed in the (X, Y, Z) coordinate system and the resulting system of equations is linearized assuming that the equilibrium plasma profiles depend only on the radial coordinate X. Moreover, each quantity $A = A(X, Y, Z, t)$ is split in between an equilibrium part $A_0(X)$ and the perturbation $\delta A(Y, Z, t) = \delta A(Z) \exp[ik_Y Y + \gamma t]$, with k_Y the poloidal wave number and γ the linear growth rate. Equilibrium gradients are defined as $\partial_X A = -A_0/L_A$, where L_A is a characteristic length associated with A_0 at $X = a$. The X dependence of δA is neglected here because $k_Y/k_X \sim \sqrt{k_Y L_n} > 1$ for both DWs and BMs [42, 67], where k_X is the radial wave number. Assuming $\phi_0 = v_{\parallel i,0} = v_{\parallel e,0} = 0$, noting that $n_0 = 1$ and $T_{e0} = 1$ in normalized units, and neglecting gyroviscous and diffusion terms, the resulting linearized system of equations is written as

$$\gamma\delta n = -ik_Y \frac{R_0}{L_n}\delta\phi - 2ik_Y \cos(\theta)\left(\delta p_e - \delta\phi\right) + \partial_Z\left(\delta j_\parallel - \delta v_{\parallel i}\right), \tag{14}$$

$$\gamma\delta\omega = -2ik_Y \cos(\theta)\delta p_e + \partial_Z \delta j_\parallel, \tag{15}$$

$$\frac{m_e}{m_i}\gamma\delta v_{\parallel e} = \partial_Z\left(\delta\phi - \delta p_e - 0.71\delta T_e\right) + \nu\delta j_\parallel, \tag{16}$$

$$\gamma\delta v_{\parallel i} = -\partial_Z \delta p_e, \tag{17}$$

$$\gamma\delta T_e = -ik_Y\eta\frac{R_0}{L_n}\delta\phi - ik_Y\frac{4\cos(\theta)}{3}\left(\delta p_e + \frac{5}{2}\delta T_e - \delta\phi\right) + \frac{2}{3}\partial_Z\left(1.71\delta j_\parallel - \delta v_{\parallel i}\right), \tag{18}$$

where $\delta p_e = \delta n + \delta T_e$, $\delta j_\parallel = \delta v_{\parallel i} - \delta v_{\parallel e}$, $\delta\omega = -k_Y^2\delta\phi$, and $\eta = L_n/L_{T_e}$. Equations (14)-(18) determine the linear growth rate of the SOL plasma instabilities.

To solve Eqs. (14)-(18), a numerical code was developed, which evaluates γ as a function of the parameters R_0/L_n, η, ν, q, and k_Y. The numerical implementation of the code is detailed in Ref. [13], and its main features are summarized here. First, the Z coordinate is discretized using a fourth order finite difference scheme. Second, Dirichlet boundary conditions are imposed at the end of the flux tube to δn, $\delta\phi$, and δT_e, while no boundary conditions are applied to the ion and electron parallel velocities. We note that we extend the simulation domain along the Z coordinate to mitigate the impact of the boundary conditions on the obtained results. Finally, the discretized system of equations is integrated implicitly in time, starting from random noise. By studying the growth of the most unstable mode, we obtain γ.

As discussed in Sec. V A, it is possible to remove the BM instability from the system, Eqs. (14)-(18), by zeroing out the curvature term in the vorticity equation, i.e. neglecting the first term of the right-hand side of Eq. (15). The solution of the resulting reduced model is denoted in the following as γ_{DW}. On the other hand, similarly to Eq. (12), DWs are removed from the model by neglecting the diamagnetic term in the Ohm's equation, i.e. zeroing out the δp_e and δT_e terms of Eq. (16). The solution of this reduced model is denoted in the following as γ_{BM}.

Considering $m_e/m_i = 800$ and the parameters ν, R_0 and q provided by experimental measurements of the plasma equilibrium, setting $\eta \simeq 0.7$ according to typical simulation results (see, e.g., Ref. [42], and also in agreement with the nonlinear results obtained with the two GBS simulations of RFX-mod), and imposing L_p and k_Y as evaluated in Sec. III from the nonlinear simulations, we solve Eqs. (14)-(18) for γ, γ_{DW}, and γ_{BM}. For the two discharges #38373 and #38413 we obtain $\gamma = 5.1, 4.4$, $\gamma_{DW} = 5.2, 4.5$, and $\gamma_{BM} = 0.3, 0.1$, respectively. While the values of γ_{DW} are similar to the growth rates obtained by solving the original Eqs. (14)-(18), removing the DWs from the system leads to a growth rate close to zero. This means that the DW is the instability that drives most of the SOL turbulent transport in the two plasma discharges considered herein, in agreement with the nonlinear results and theoretical expectations.

In order to disentangle the impact of resistivity and electron inertia on DWs, we simplify Eqs. (14)-(18) as follows. We first neglect the curvature terms to avoid coupling with BMs, together with the compressibility terms in the continuity and temperature equations. Then, assuming $\gamma \gg k_Z$, we remove the sound wave coupling from the model. The resulting system of equations is written as

$$\gamma \delta n = -ik_Y \frac{R_0}{L_n} \delta\phi - \partial_Z \delta v_{\parallel e}, \tag{19}$$

$$\gamma \delta\omega = -\partial_Z \delta v_{\parallel e}, \tag{20}$$

$$\frac{m_e}{m_i} \gamma \delta v_{\parallel e} = \partial_Z \left(\delta\phi - \delta p_e - 0.71 \delta T_e\right) - \nu \delta v_{\parallel e}, \tag{21}$$

$$\gamma \delta T_e = -ik_Y \eta \frac{R_0}{L_n} \delta\phi - 1.71 \frac{2}{3} \partial_Z \delta v_{\parallel e}. \tag{22}$$

Equations (19)-(22) constitute the minimal model necessary to describe the linear dynamics of RDWs and InDWs. RDWs and InDWs are removed from the model, Eqs. (19)-(22), by setting $\nu = 0$ and $m_e/m_i = 0$, respectively. Solving Eqs. (19)-(22) for the two plasma

discharges #38373 and #38413 with the linear code discussed above, we obtain respectively $\gamma = 6.1, 4.7$ for $\nu = 0$ and $\gamma = 3.1, 1.9$ for $m_e/m_i = 0$. Since the growth rates are approximatively a factor two smaller for $m_e/m_i = 0$ with respect to $\nu = 0$, we conclude that InDWs are driving most of the SOL turbulent transport in the two plasma discharges considered here, in agreement with the conclusions in Ref. [12].

We note that, while k_Y and L_n, input of the linear code, can be obtained from the nonlinear simulation results, they can also be estimated semi-analytically. In fact, in the limit of a negligible $\mathbf{E} \times \mathbf{B}$ shear flow, the saturation of the growth of BMs and DWs is usually determined by the gradient removal mechanism, i.e. the saturation of the mode is due to the nonlinear local flattening of the plasma pressure profile, thus removing the drive of the instability [14]. The main aspects of this theory are detailed in Appendix A and the main result is

$$L_p = \frac{L_n}{1+\eta} = \frac{q}{c_s}\left(\frac{\gamma}{k_Y}\right)_{\max}, \tag{23}$$

with $c_s = 1$ because of the normalization employed. Equation (23) is an implicit equation for L_n, that is solved by scanning γ, solution of Eqs. (14)-(18), over the parameter space (k_Y, L_n) and searching for the values of L_n and k_Y that satisfy Eq. (23). This procedure is applied to determine the equilibrium pressure gradient length of the two plasma discharges #38373 and #38413 for $m_i/m_e = 800$, obtaining $L_p = 44, 56$, $k_Y = 0.17, 0.17$, and $\gamma = 3.8, 3.1$, respectively. The L_p values computed according to Eq. (23) are in qualitative agreement with the results obtained from the nonlinear simulations discussed in Sec. III. Moreover, the poloidal wave number, k_Y, associated with the instability that drives most of the SOL turbulent transport is in good quantitative agreement with the nonlinear results.

Equation (23) allows us to investigate the impact of the reduced ion to electron mass ratio on our results. This is necessary since performing nonlinear simulations with $m_i/m_e = 3600$ is too demanding in terms of computational resources. Imposing a realistic ion to electron mass ratio $m_i/m_e = 3600$, Eq. (23) gives $L_p = 39, 52$ and $k_Y = 0.14, 0.16$ for the two considered plasma discharges. We see that L_p and k_Y are only slightly affected by increasing the ion to electron mass ratio to a realistic value. Using these L_p and k_Y as input parameters, we solve Eqs. (14)-(18) with $m_i/m_e = 3600$, thus obtaining for the two considered discharges $\gamma = 2.8$, $\gamma_{DW} = 2.9$ and $\gamma_{BM} = 0.1$. Moreover, solving Eqs. (19)-(22) for γ with L_p and k_Y computed according to Eq. (23), we obtain $\gamma = 4.6, 3.7$ for $\nu = 0$ and the realistic $m_i/m_e = 3600$, while we have $\gamma = 2.4, 1.5$ for $m_i/m_e = 0$. Therefore, we conclude that the same turbulent

regime obtained with $m_i/m_e = 800$ is found also for the realistic $m_i/m_e = 3600$, i.e. the SOL turbulent transport is mainly driven by InDWs.

VI. CONCLUSIONS

In the present paper GBS simulations based on two RFX-mod plasma discharges with low edge safety factors are discussed. The GBS simulations are compared with experimental measurements, showing good qualitative and quantitative agreement for most of the considered quantities. Moreover, the SOL turbulent regime in the two discharges is identified.

The nonlinear simulations, carried out with GBS, are based on the two RFX-mod plasma discharges #38373 and #38413. In order to expand the GBS validation parameter regime and assess the reliability of the GBS model at low safety factor values, the simulation results are carefully compared with experimental measurements. It is found that the numerical results are in good agreement with experimental radial equilibrium profiles, fluctuation measurements, and higher order moments of j_{sat} and V_{fl}, except for the equilibrium profile of V_{fl} and the level of fluctuations of j_{sat}. We infer that the observed discrepancies between simulations and experimental measurements are, at least in part, related to simulating only the tokamak SOL region, without including the plasma dynamics inside the LCFS, and to the limits of applicability of the drift reduced approximation.

For the two considered discharges, the simulation results indicate that the turbulent transport is mostly driven by DWs. To disentangle the effect of resistivity and electron inertia on the RFX-mod SOL dynamics, a linear model is introduced. It is found that plasma adiabaticity is mostly broken by electron inertia, resulting in InDWs. Moreover, assuming that the linear growth of BMs and DWs saturates because of the nonlinear local flattening of the plasma pressure profile, the equilibrium pressure gradient length and the wave number associated with the instability that drives most of the turbulence transport are estimated with a quasi-linear theory, showing good agreement with the nonlinear results. This theory is then employed to investigate the impact of the reduced ion to electron mass that is used in the nonlinear simulations. It is found that InDWs are expected to drive the SOL turbulence also for the realistic $m_i/m_e = 3600$.

Acknowledgments

The simulations presented herein were carried out in part using the HELIOS supercomputer system at Computational Simulation Centre of International Fusion Energy Research Center (IFERC-CSC), Aomori, Japan, under the Broader Approach collaboration between Euratom and Japan, implemented by Fusion for Energy and JAEA; in part at the Swiss National Supercomputing Center (CSCS) under Projects ID s549, s655, and s718; and in part on the CINECA Marconi supercomputer within the framework of the GBSSOL project. This work has been carried out within the framework of the EUROfusion Consortium and has received funding from the Fond National Suisse de la Recherche scientifique and from the Euratom research and training programme 2014-2018 under grant agreement No 633053. The views and opinions expressed herein do not necessarily reflect those of the European Commission.

APPENDIX A: ESTIMATE OF THE EQUILIBRIUM PRESSURE GRADIENT LENGTH

The time-averaged plasma pressure gradient scale length $L_p = -p_e/\nabla p_e$ in the tokamak SOL originates from a balance between the turbulent perpendicular transport of particles and heat, resulting from the nonlinear development of the unstable modes, and the parallel losses at the end of the magnetic field lines. In the limit of a negligible $\mathbf{E} \times \mathbf{B}$ shear flow and for typical SOL parameters, it is typically justified to assume that the gradient removal turbulence saturation mechanism, i.e. the local nonlinear flattening of the plasma pressure profile and the resulting removal of the instability drive, is the mechanism that regulates the amplitude of SOL turbulence [14].

The main features of the theory are summarized here. The fundamental hypothesis is that the saturation of the growth rate of the linear modes occurs when these are able to remove their own drive, namely, the amplitude of the gradient associated with the fluctuation, $k_X \delta p_e$, is comparable to the gradient of the background pressure, p_{e0}/L_p ($k_X \sim \sqrt{k_Y/L_p}$ is the radial extension of BMs or DWs obtained from a non-local linear theory [42, 67]). This provides an estimate for the amplitude of the fluctuations $\delta p_e = p_{e0}/\sqrt{k_Y L_p}$. Then, the leading terms in the linearized pressure continuity equation,

$$\gamma \delta p_e + R_0 k_Y \delta\phi \frac{p_{e0}}{L_p} \simeq 0, \tag{A1}$$

provide an estimate of the electromagnetic potential fluctuations $\delta\phi \sim \gamma\delta p_e L_p/(R_0 p_{e0} k_Y)$ and therefore of the turbulent $\mathbf{E}\times\mathbf{B}$ flux, $\Gamma = k_Y\delta\phi\delta p_e \sim \gamma p_{e0}/(R_0 k_Y)$. Finally, the balance between the perpendicular turbulent transport, $R_0\partial_X\Gamma \sim R_0\Gamma/L_p \sim \gamma p_{e0}/(k_Y L_p)$, and the parallel losses at the end of magnetic field lines, $\nabla_\parallel(p_e v_{\parallel e}) \sim p_{e0}c_s/q$, gives

$$L_p = \frac{q}{c_s}\left(\frac{\gamma}{k_Y}\right)_{\max}, \tag{A2}$$

where γ/k_Y should be maximized over the unstable modes present in the system.

---

[1] A. Loarte, B. Lipschultz, A. S. Kukushkin, G. F. Matthews, P. C. Stangeby, N. Asakura, G. F. Counsell, G. Federici, A. Kallenbach, K. Krieger, A. Mahdavi, V. Philipps, D. Reiter, J. Roth, J. Strachan, D. Whyte, R. Doerner, T. Eich, W. Fundamenski, A. Herrmann, M. Fenstermacher, P. Ghendrih, M. Groth, A. Kirschner, S. Konoshima, B. LaBombard, P. Lang, A. W. Leonard, P. Monier-Garbet, R. Neu, H. Pacher, B. Pegourie, R. A. Pitts, S. Takamura, J. Terry, E. Tsitrone, t. I. S.-o. L. Group, and Diver. Chapter 4: Power and particle control. *Nuclear Fusion* **47**, S203–S263 (2007).

[2] B. D. Dudson, M. V. Umansky, X. Q. Xu, P. B. Snyder, and H. R. Wilson. BOUT++: A framework for parallel plasma fluid simulations. *Computer Physics Communications* **180**, 1467–1480 (2009).

[3] P. Ricci, F. D. Halpern, S. Jolliet, J. Loizu, A. Mosetto, A. Fasoli, I. Furno, and C. Theiler. Simulation of plasma turbulence in scrape-off layer conditions: the GBS code, simulation results and code validation. *Plasma Physics and Controlled Fusion* **54**, 124047 (2012).

[4] J. J. Rasmussen, A. H. Nielsen, J. Madsen, V. Naulin, and G. S. Xu. Numerical modeling of the transition from low to high confinement in magnetically confined plasma. *Plasma Physics and Controlled Fusion* **58**, 014031 (2016).

[5] P. Tamain, H. Bufferand, G. Ciraolo, C. Colin, P. Ghendrih, F. Schwander, and E. Serre. 3D Properties of Edge Turbulent Transport in Full-Torus Simulations and their Impact on Poloidal Asymmetries. *Contributions to Plasma Physics* **54**, 555–559 (2014).

[6] E. J. Doyle (Chair Transport Physics), W. A. Houlberg (Chair Confinement Database and Modelling), Y. Kamada (Chair Pedestal and Edge), V. Mukhovatov (co-Chair Transport Physics), T. H. Osborne (co-Chair Pedestal and Edge), A. Polevoi (co-Chair Confinement

Database and Modelling), G. Bateman, J. W. Connor, J. G. Cordey (retired), T. Fujita, X. Garbet, T. S. Hahm, L. D. Horton, A. E. Hubbard, F. Imbeaux, F. Jenko, J. E. Kinsey, Y. Kishimoto, J. Li, T. C. Luce, Y. Martin, M. Ossipenko, V. Parail, A. Peeters, T. L. Rhodes, J. E. Rice, C. M. Roach, V. Rozhansky, F. Ryter, G. Saibene, R. Sartori, A. C. C. Sips, J. A. Snipes, M. Sugihara, E. J. Synakowski, H. Takenaga, T. Takizuka, K. Thomsen, M. R. Wade, H. R. Wilson, ITPA Transport Physics Topical Group, ITPA Confinement Database and Modelling Topical Group, and ITPA Pedestal and Edge Topical Group. Chapter 2: Plasma confinement and transport. *Nuclear Fusion* **47**, S18 (2007).

[7] R. Pitts, S. Carpentier, F. Escourbiac, T. Hirai, V. Komarov, A. Kukushkin, S. Lisgo, A. Loarte, M. Merola, R. Mitteau, A. Raffray, M. Shimada, and P. Stangeby. Physics basis and design of the ITER plasma-facing components. *Journal of Nuclear Materials* **415**, S957–S964 (2011).

[8] G. Arnoux, T. Farley, C. Silva, S. Devaux, M. Firdaouss, D. Frigione, R. Goldston, J. Gunn, J. Horacek, S. Jachmich, P. Lomas, S. Marsen, G. Matthews, R. Pitts, M. Stamp, and P. Stangeby. Scrape-off layer properties of ITER-like limiter start-up plasmas in JET. *Nuclear Fusion* **53**, 073016 (2013).

[9] A. Zeiler, D. Biskamp, J. F. Drake, and P. N. Guzdar. Three-dimensional fluid simulations of tokamak edge turbulence. *Physics of Plasmas* **3**, 2951–2960 (1996).

[10] B. D. Scott. Drift wave versus interchange turbulence in tokamak geometry: Linear versus nonlinear mode structure. *Physics of Plasmas* **12**, 062314 (2005).

[11] T. Rafiq, G. Bateman, A. H. Kritz, and A. Y. Pankin. Development of drift-resistive-inertial ballooning transport model for tokamak edge plasmas. *Physics of Plasmas* **17**, 082511 (2010).

[12] A. Mosetto, F. D. Halpern, S. Jolliet, J. Loizu, and P. Ricci. Turbulent regimes in the tokamak scrape-off layer. *Physics of Plasmas* **20**, 092308 (2013).

[13] A. Mosetto, F. D. Halpern, S. Jolliet, and P. Ricci. Low-frequency linear-mode regimes in the tokamak scrape-off layer. *Physics of Plasmas* **19**, 112103 (2012).

[14] P. Ricci and B. N. Rogers. Plasma turbulence in the scrape-off layer of tokamak devices. *Physics of Plasmas* **20**, 010702 (2013).

[15] O. Garcia, J. Horacek, R. Pitts, A. Nielsen, W. Fundamenski, V. Naulin, and J. J. Rasmussen. Fluctuations and transport in the TCV scrape-off layer. *Nuclear Fusion* **47**, 667–676 (2007).

[16] F. Militello, W. Fundamenski, V. Naulin, and A. H. Nielsen. Simulations of edge and scrape off

layer turbulence in mega ampere spherical tokamak plasmas. *Plasma Physics and Controlled Fusion* **54**, 095011 (2012).

[17] N. Yan, A. H. Nielsen, G. S. Xu, V. Naulin, J. J. Rasmussen, J. Madsen, H. Q. Wang, S. C. Liu, W. Zhang, L. Wang, and B. N. Wan. Statistical characterization of turbulence in the boundary plasma of EAST. *Plasma Physics and Controlled Fusion* **55**, 115007 (2013).

[18] F. D. Halpern, J. L. Terry, S. J. Zweben, B. LaBombard, M. Podesta, and P. Ricci. Comparison of 3D flux-driven scrape-off layer turbulence simulations with gas-puff imaging of Alcator C-Mod inner-wall limited discharges. *Plasma Physics and Controlled Fusion* **57**, 054005 (2015).

[19] F. Nespoli, I. Furno, F. Halpern, B. Labit, J. Loizu, P. Ricci, and F. Riva. Non-linear simulations of the TCV Scrape-Off Layer. *Nuclear Materials and Energy* **0**, 1–4 (2016).

[20] R. Jorge, P. Ricci, F. D. Halpern, N. F. Loureiro, and C. Silva. Plasma turbulence in the scrape-off layer of the ISTTOK tokamak. *Physics of Plasmas* **23**, 102511 (2016).

[21] P. Tamain, H. Bufferand, G. Ciraolo, C. Colin, D. Galassi, P. Ghendrih, F. Schwander, and E. Serre. The TOKAM3X code for edge turbulence fluid simulations of tokamak plasmas in versatile magnetic geometries. *Journal of Computational Physics* **321**, 606–623 (2016).

[22] F. D. Halpern, P. Ricci, B. Labit, I. Furno, S. Jolliet, J. Loizu, A. Mosetto, G. Arnoux, J. P. Gunn, J. Horacek, M. Kočan, B. LaBombard, and C. Silva. Theory-based scaling of the SOL width in circular limited tokamak plasmas. *Nuclear Fusion* **53**, 122001 (2013).

[23] F. D. Halpern, P. Ricci, S. Jolliet, J. Loizu, and A. Mosetto. Theory of the scrape-off layer width in inner-wall limited tokamak plasmas. *Nuclear Fusion* **54**, 043003 (2014).

[24] F. D. Halpern, J. Horacek, R. A. Pitts, and P. Ricci. A theoretical interpretation of the main scrape-off layer heat-flux width scaling for tokamak inner-wall limited plasmas. *Plasma Physics and Controlled Fusion* **58**, 084003 (2016).

[25] P. Sonato, R. Piovan, and A. Luchetta. Control of non-axisymmetric magnetic fields for plasma enhanced performances: The RFX contribution. *Fusion Engineering and Design* **74**, 97–107 (2005).

[26] P. Martin, J. Adamek, P. Agostinetti, M. Agostini, A. Alfier, C. Angioni, V. Antoni, L. Apolloni, F. Auriemma, O. Barana, S. Barison, M. Baruzzo, P. Bettini, M. Boldrin, T. Bolzonella, D. Bonfiglio, F. Bonomo, A. Boozer, M. Brombin, J. Brotankova, A. Buffa, A. Canton, S. Cappello, L. Carraro, R. Cavazzana, M. Cavinato, L. Chacon, G. Chitarin, W. Cooper, S. D. Bello, M. Dalla Palma, R. Delogu, A. De Lorenzi, G. De Masi, J. Dong, M. Drevlak, D. Es-

cande, F. Fantini, A. Fassina, F. Fellin, A. Ferro, S. Fiameni, A. Fiorentin, P. Franz, E. Gaio, X. Garbet, E. Gazza, L. Giudicotti, F. Gnesotto, M. Gobbin, L. Grando, S. Guo, Y. Hirano, S. Hirshman, S. Ide, V. Igochine, Y. In, P. Innocente, S. Kiyama, S. Liu, Y. Liu, D. Lòpez Bruna, R. Lorenzini, A. Luchetta, G. Manduchi, D. Mansfield, G. Marchiori, D. Marcuzzi, L. Marrelli, S. Martini, G. Matsunaga, E. Martines, G. Mazzitelli, K. McCollam, S. Menmuir, F. Milani, B. Momo, M. Moresco, S. Munaretto, L. Novello, M. Okabayashi, S. Ortolani, R. Paccagnella, R. Pasqualotto, M. Pavei, G. Perverezev, S. Peruzzo, R. Piovan, P. Piovesan, L. Piron, A. Pizzimenti, N. Pomaro, N. Pomphrey, I. Predebon, M. Puiatti, V. Rigato, A. Rizzolo, G. Rostagni, G. Rubinacci, A. Ruzzon, H. Sakakita, R. Sanchez, J. Sarff, F. Sattin, A. Scaggion, P. Scarin, W. Schneider, G. Serianni, P. Sonato, E. Spada, A. Soppelsa, S. Spagnolo, M. Spolaore, D. Spong, G. Spizzo, M. Takechi, C. Taliercio, D. Terranova, V. Toigo, M. Valisa, M. Veranda, N. Vianello, F. Villone, Z. Wang, R. White, D. Yadikin, P. Zaccaria, A. Zamengo, P. Zanca, B. Zaniol, L. Zanotto, E. Zilli, G. Zollino, and M. Zuin. Overview of the RFX fusion science program. *Nuclear Fusion* **51**, 094023 (2011).

[27] P. Piovesan, D. Bonfiglio, F. Auriemma, F. Bonomo, L. Carraro, R. Cavazzana, G. De Masi, A. Fassina, P. Franz, M. Gobbin, L. Marrelli, P. Martin, E. Martines, B. Momo, L. Piron, M. Valisa, M. Veranda, N. Vianello, B. Zaniol, M. Agostini, M. Baruzzo, T. Bolzonella, A. Canton, S. Cappello, L. Chacón, G. Ciaccio, D. F. Escande, P. Innocente, R. Lorenzini, R. Paccagnella, M. E. Puiatti, P. Scarin, A. Soppelsa, G. Spizzo, M. Spolaore, D. Terranova, P. Zanca, L. Zanotto, and M. Zuin. RFX-mod: A multi-configuration fusion facility for three-dimensional physics studies. *Physics of Plasmas* **20**, 056112 (2013).

[28] M. Spolaore, R. Cavazzana, L. Marrelli, L. Carraro, P. Franz, S. Spagnolo, B. Zaniol, M. Zuin, L. Cordaro, S. D. Bello, G. D. Masi, A. Ferro, C. Finotti, L. Grando, P. Innocente, O. Kudlacek, G. Marchiori, E. Martines, B. Momo, R. Paccagnella, P. Piovesan, C. Piron, M. E. Puiatti, M. Recchia, P. Scarin, C. Taliercio, N. Vianello, and L. Zanotto. H-mode Achievement and Edge Features in RFX-mod Tokamak Operation. *26th IAEA Fusion Energy Conference*, EX/P5–24. Kyoto, Japan (2016).

[29] M. Spolaore, N. Vianello, M. Agostini, R. Cavazzana, E. Martines, G. Serianni, P. Scarin, E. Spada, M. Zuin, and V. Antoni. Magnetic and electrostatic structures measured in the edge region of the RFX-mod experiment. *Journal of Nuclear Materials* **390-391**, 448–451 (2009).

[30] N. Vianello, M. Spolaore, E. Martines, R. Cavazzana, G. Serianni, M. Zuin, E. Spada, and V. Antoni. Drift-Alfvén vortex structures in the edge region of a fusion relevant plasma. *Nuclear Fusion* **50**, 042002 (2010).

[31] H. Y. W. Tsui, R. D. Bengtson, G. X. Li, H. Lin, M. Meier, C. P. Ritz, and A. J. Wootton. A new scheme for Langmuir probe measurement of transport and electron temperature fluctuations. *Review of Scientific Instruments* **63**, 4608–4610 (1992).

[32] S. I. Braginskii. Transport Processes in a Plasma. *Reviews of Plasma Physics* **1**, 205 (1965).

[33] A. Zeiler, J. F. Drake, and B. Rogers. Nonlinear reduced Braginskii equations with ion thermal dynamics in toroidal plasma. *Physics of Plasmas* **4**, 2134 (1997).

[34] F. D. Halpern, S. Jolliet, J. Loizu, A. Mosetto, and P. Ricci. Ideal ballooning modes in the tokamak scrape-off layer. *Physics of Plasmas* **20**, 052306 (2013).

[35] S. Jolliet, F. D. Halpern, J. Loizu, A. Mosetto, and P. Ricci. Aspect ratio effects on limited scrape-off layer plasma turbulence. *Physics of Plasmas* **21**, 022303 (2014).

[36] A. Mosetto, F. D. Halpern, S. Jolliet, J. Loizu, and P. Ricci. Finite ion temperature effects on scrape-off layer turbulence. *Physics of Plasmas* **22**, 012308 (2015).

[37] D. A. Russell, D. A. D'Ippolito, and J. R. Myra. On relaxing the Boussinesq approximation in scrape-off layer turbulence (SOLT) model simulations. *Bulletin of the American Physical Society, 54th Annual Meeting of the APS Division of Plasma Physics*, vol 57, BP8.159. Providence, Rhode Island, USA (2012).

[38] G. Q. Yu, S. I. Krasheninnikov, and P. N. Guzdar. Two-dimensional modelling of blob dynamics in tokamak edge plasmas. *Physics of Plasmas* **13**, 042508 (2006).

[39] K. Bodi, G. Ciraolo, P. Ghendrih, F. Schwander, E. Serre, and P. Tamain. Impact of the Boussinesq approximation in tokamak scrape–off layer turbulence. *38th EPS Conference on Plasma Physics*, P1.121. Strasbourg, France (2011).

[40] F. D. Halpern, P. Ricci, S. Jolliet, J. Loizu, J. Morales, A. Mosetto, F. Musil, F. Riva, T. M. Tran, and C. Wersal. The GBS code for tokamak scrape-off layer simulations. *Journal of Computational Physics* **315**, 388–408 (2016).

[41] B. N. Rogers and P. Ricci. Low-Frequency Turbulence in a Linear Magnetized Plasma. *Physical Review Letters* **104**, 225002 (2010).

[42] P. Ricci, B. N. Rogers, and S. Brunner. High- and Low-Confinement Modes in Simple Magnetized Toroidal Plasmas. *Physical Review Letters* **100**, 225002 (2008).

[43] P. Ricci and B. N. Rogers. Transport scaling in interchange-driven toroidal plasmas. *Physics of Plasmas* **16**, 062303 (2009).

[44] P. Ricci and B. N. Rogers. Turbulence Phase Space in Simple Magnetized Toroidal Plasmas. *Physical Review Letters* **104**, 145001 (2010).

[45] J. Loizu, P. Ricci, F. D. Halpern, and S. Jolliet. Boundary conditions for plasma fluid models at the magnetic presheath entrance. *Physics of Plasmas* **19**, 122307 (2012).

[46] A. Arakawa. Computational design for long-term numerical integration of the equations of fluid motion: Two-dimensional incompressible flow. Part I. *Journal of Computational Physics* **1**, 119–143 (1966).

[47] F. Riva, P. Ricci, F. D. Halpern, S. Jolliet, J. Loizu, and A. Mosetto. Verification methodology for plasma simulations and application to a scrape-off layer turbulence code. *Physics of Plasmas* **21**, 062301 (2014).

[48] C. K. Tsui, J. A. Boedo, F. D. Halpern, J. Loizu, F. Nespoli, J. Horacek, B. Labit, J. Morales, H. Reimerdes, P. Ricci, C. Theiler, S. Coda, B. P. Duval, and I. Furno. Poloidal asymmetry in the narrow heat flux feature in the TCV scrape-off layer. *Physics of Plasmas* **24**, 062508 (2017).

[49] F. Halpern and P. Ricci. Velocity shear, turbulent saturation, and steep plasma gradients in the scrape-off layer of inner-wall limited tokamaks. *Nuclear Fusion* **57**, 034001 (2017).

[50] E. Sánchez, C. Hidalgo, D. López-Bruna, I. García-Cortés, R. Balbín, M. A. Pedrosa, B. van Milligen, C. Riccardi, G. Chiodini, J. Bleuel, M. Endler, B. A. Carreras, and D. E. Newman. Statistical characterization of fluctuation wave forms in the boundary region of fusion and nonfusion plasmas. *Physics of Plasmas* **7**, 1408–1416 (2000).

[51] Y. H. Xu, S. Jachmich, R. R. Weynants, and t. T. Team. On the properties of turbulence intermittency in the boundary of the TEXTOR tokamak. *Plasma Physics and Controlled Fusion* **47**, 1841–1855 (2005).

[52] I. Nanobashvili, J. Gunn, and P. Devynck. Radial profiles of plasma turbulent fluctuations in the scrape-off layer of the Tore Supra tokamak. *Journal of Nuclear Materials* **363-365**, 622–627 (2007).

[53] P. Ricci, C. Theiler, A. Fasoli, I. Furno, B. Labit, S. H. Muller, M. Podesta, and F. M. Poli. Langmuir probe-based observables for plasma-turbulence code validation and application to the TORPEX basic plasma physics experiment. *Physics of Plasmas* **16**, 055703 (2009).

[54] H. Wang, G. Xu, H. Guo, B. Wan, V. Naulin, S. Ding, N. Yan, W. Zhang, L. Wang, S. Liu, R. Chen, L. Shao, H. Xiong, P. Liu, M. Jiang, and G.-N. Luo. Observation of a new turbulence-driven limit-cycle state in H-modes with lower hybrid current drive and lithium-wall conditioning in the EAST superconducting tokamak. *Nuclear Fusion* **52**, 123011 (2012).

[55] C. P. Ritz, E. J. Powers, T. L. Rhodes, R. D. Bengtson, K. W. Gentle, H. Lin, P. E. Phillips, A. J. Wootton, D. L. Brower, N. C. Luhmann, W. A. Peebles, P. M. Schoch, and R. L. Hickok. Advanced plasma fluctuation analysis techniques and their impact on fusion research (invited). *Review of Scientific Instruments* **59**, 1739–1744 (1988).

[56] C. A. F. Varandas, J. A. C. Cabral, J. T. Mendonça, M. P. Alonso, P. Amorim, B. B. Carvalho, C. Correia, L. Cupido, M. L. Carvalho, J. M. Dias, H. Fernandes, C. J. Freitas, S. Magalhães, A. Malaquias, M. E. Manso, A. Praxedes, J. Santana, F. Serra, A. Silva, A. Soares, J. Sousa, W. van Toledo, P. Vaessen, P. Varela, S. Vergamota, and B. de Groot. Engineering Aspects of the Tokamak ISTTOK. *Fusion Technology* **29**, 105–115 (1996).

[57] T. T. Ribeiro and B. Scott. Gyrofluid turbulence studies of the effect of the poloidal position of an axisymmetric Debye sheath. *Plasma Physics and Controlled Fusion* **50**, 055007 (2008).

[58] J. W. Connor, R. J. Hastie, and J. B. Taylor. Shear, Periodicity, and Plasma Ballooning Modes. *Physical Review Letters* **40**, 396–399 (1978).

[59] G. Bateman and D. B. Nelson. Resistive-Ballooning-Mode Equation. *Physical Review Letters* **41**, 1804–1807 (1978).

[60] D. R. McCarthy, P. N. Guzdar, J. F. Drake, T. M. Antonsen, and A. B. Hassam. Stability of resistive and ideal ballooning modes in the Texas Experimental Tokamak and DIII-D. *Physics of Fluids B: Plasma Physics* **4**, 1846 (1992).

[61] S. V. Novakovskii, P. N. Guzdar, J. F. Drake, C. S. Liu, and F. L. Waelbroeck. New unstable branch of drift resistive ballooning modes in tokamaks. *Physics of Plasmas* **2**, 781 (1995).

[62] K. Mima and A. Hasegawa. Nonlinear instability of electromagnetic drift waves. *Physics of Fluids* **21**, 81 (1978).

[63] M. Wakatani and A. Hasegawa. A collisional drift wave description of plasma edge turbulence. *Physics of Fluids* **27**, 611 (1984).

[64] H. Sugama, M. Wakatani, and A. Hasegawa. Study of resistive drift and resistive interchange modes in a cylindrical plasma with magnetic shear. *Physics of Fluids* **31**, 1601 (1988).

[65] W. Horton. Drift waves and transport. *Reviews of Modern Physics* **71**, 735–778 (1999).

[66] P. H. Diamond, A. Hasegawa, and K. Mima. Vorticity dynamics, drift wave turbulence, and zonal flows: a look back and a look ahead. *Plasma Physics and Controlled Fusion* **53**, 124001 (2011).

[67] B. N. Rogers and W. Dorland. Noncurvature-driven modes in a transport barrier. *Physics of Plasmas* **12**, 062511 (2005).